Excitation and nonradiative deexcitation processes of Er^{3+} in crystalline Si

Francesco Priolo
Istituto Nazionale per la Fisica della Materia and Dipartimento di Fisica, Università di Catania, Corso Italia 57, I 95129 Catania, Italy

Giorgia Franzò and Salvatore Coffa
Istituto Nazionale di Metodologie e Tecnologie per la Microelettronica, Consiglio Nazionale delle Ricerche, Stradale Primosole 50, I 95121 Catania, Italy

Alberto Carnera
Istituto Nazionale per la Fisica della Materia and Dipartimento di Fisica ''Galileo Galilei,'' Università di Padova, Via F. Marzolo 8, I 35131 Padova, Italy

(Received 1 August 1997)

A detailed investigation on the excitation and deexcitation processes of Er^{3+} in Si is reported. In particular, we explored Er pumping through electron-hole pair recombination and Er deexcitation through Auger processes transferring energy to either free or bound electrons and holes. Since Er donor behavior would result in a free-carrier concentration varying along its profile, experiments have been performed by embedding the whole Er profile within previously prepared *n*-doped or *p*-doped regions. Multiple P (B) implants were performed in *n*-type (*p*-type) Czochralski Si samples in order to realize uniform dopant concentrations from 4×10^{16} to $1.2\times10^{18}/cm^3$ at depths between 0.5 and 2.5 μm below the surface. These samples have been subsequently implanted with 4 MeV 3.3×10^{13} Er/cm^2 and annealed at 900 °C for 30 min. Free electrons or holes concentrations in the region where Er sits were measured by spreading resistance profiling. It has been found that the release of electrons or holes from shallow donors and acceptors, occurring at temperatures between 15 and 100 K, produces a strong reduction of both time decay and luminescence intensity at 1.54 μm. These phenomena are produced by Auger deexcitation of the Er^{3+} intra-4*f* electrons with energy transfer to free carriers. The Auger coefficient of this process has been measured to be $C_A\sim5\times10^{-13}$ cm^3 s^{-1} for both free electrons and free holes. Moreover, at 15 K (when the free carriers are frozen and the donor and acceptor levels occupied) the Er^{3+} time decay has been found to depend on the P (or B) concentrations. This is attributed to an impurity Auger deexcitation to electrons (or holes) bound to shallow donors (acceptors): the efficiency of this process has been determined to be two orders of magnitude smaller with respect to the Auger deexcitation with free carriers. Furthermore, at temperatures above 100 K a nonradiative back-transfer decay process, characterized by an activation energy of 0.15 eV, is seen to set in for both *p*-type and *n*-type samples. This suggests that the back-transfer process, which severely limits the high-temperature luminescence efficiency, is always completed by a thermalization of an electron trapped at an Er-related level to the conduction band. Finally, by analysis of the pump power dependence of time decay and luminescence yield at 15 K, we have found that excitation of Er through the recombination of an electron-hole pair is a very efficient process, characterized by an effective cross section of 3×10^{-15} cm^2 and able to provide an internal quantum efficiency as high as 10% at low temperatures (15 K) and pump powers (below 1 mW). This efficiency is significantly reduced when, at higher temperatures and/or high pump powers, strong nonradiative decay processes set in. These phenomena are investigated in detail and their impact on device operation perspectives are analyzed and discussed. [S0163-1829(98)01008-X]

I. INTRODUCTION

Silicon is the leading semiconductor in the microelectronic industry. In fact, due to its mature processing technology and to the continuous improvements in the scale integration, this semiconductor is able to satisfy the increasing demand for higher complexity integrated circuits. There is no doubt that the silicon technology will dominate the semiconductor market for at least two more decades. At the same time optoelectronics, especially optocommunication, has entered a long term growth phase. Due to its indirect band gap and to the absence of linear electro-optic effects, Si has been considered unsuitable for optoelectronic applications that remain the domain of III-V semiconductors and glass fibers. Several applications, such as optical interconnections at the chip-to-chip level, require integration of electrical and optical functions on the same device.[1] One way to fulfill these requirements is to combine the optical properties of III-Vs with the electronic performances of crystalline silicon through an hybrid integration. Alternatively, several approaches have been undertaken to circumvent the physical inability of Si to act as a light source.[2] Among them porous Si,[3] Si-rich silicon oxide,[4] $Si_{1-x}Ge_x$ heteroepitaxy on Si (Ref. 5) and rare-earth doping of Si (Refs. 6 and 7) have been considered so far the most successful.

In particular, Er doping of Si has recently emerged as a quite promising route towards Si-based optoelectronics.[6–34] Erbium is a rare earth, which, in its 3+ state, is characterized

by a radiative intra-$4f$ shell atomiclike transition emitting photons at 1.54 μm, a wavelength that is strategic in telecommunication technology since it matches a window of maximum transmission for the silica optical fibers. The introduction of Er in Si would in principle allow electronic excitation of the $4f$ transition through a carrier-mediated process with a subsequent radiative deexcitation. Indeed, the first Er-doped light-emitting diode (LED) operating at 1.54 μm has been demonstrated more than one decade ago[9] at 77 K. However, the achievement of room-temperature light emission has been hampered for a long time by a strong temperature quenching. The important potential applications of this process have driven worldwide an increasing interest on the understanding of the Si: Er system and we have now gained a huge amount of information leading to the fabrication of room-temperature operating LED's.[10–13] For instance, we have learned that O or F co-doping produces Er-impurity complexes,[14–16] avoids Er precipitation and segregation,[17,18] enhances the Er luminescence,[15,19] and reduces its quenching,[20] modifies the deep-level properties of Er in Si,[21,22] and produces a donor behavior.[23] Moreover, the excitation and deexcitation processes of Er in Si have been investigated. It has been shown that in photoluminescence (PL) Er is excited through the recombination of photogenerated carriers at a deep level introduced by Er in the band gap of Si (probably a level at 0.15 eV from the conduction band is responsible for excitation).[19,24] In a diode structure under forward bias the Er excitation process is the same as in PL while under reverse bias excitation is produced by impact of hot carriers within the depletion region of the device.[25] Once excited deexcitation can occur either radiatively (with a lifetime of about 2 ms) or through competing nonradiative paths. An understanding and control of the competing nonradiative deexcitation routes represent a crucial step towards the improvement of luminescence efficiencies.

Among the different nonradiative processes the back transfer and the impurity Auger with free carriers have been recently recognized as the most important decay processes in competition with spontaneous radiative emission.[20,26–27] The back transfer process is schematically depicted in Fig. 1(a): the excited electron in the $4f$ shell of the Er^{3+} ion can decay nonradiatively by promoting an electron from the valence band to an Er-related level in the Si band gap. Note that this process is exactly the reverse of excitation, hence the name back transfer since the energy is transferred back through the same path. The extra energy required to complete this process (ΔE) is given by phonons, hence this deexcitation is expected to be thermally activated. Moreover, it is necessary that the Er-related level is empty to allow the promotion of an electron: therefore the occupation probability of this level, i.e., the position of the Fermi level, should play a crucial role in determining the effectiveness of this process. The Auger impurity deexcitation with free carriers is depicted in Figs. 1(b) and 1(c) for electrons and holes, respectively. In this case deexcitation of the excited $4f$ electron occurs by giving the energy to an electron in the conduction band or to a hole in the valence band. This process resembles the opposite of impact excitation from hot carriers. Deexcitation probability is proportional to the concentration of free electrons (or free holes) and hence also this process depends on the position of the Fermi level.

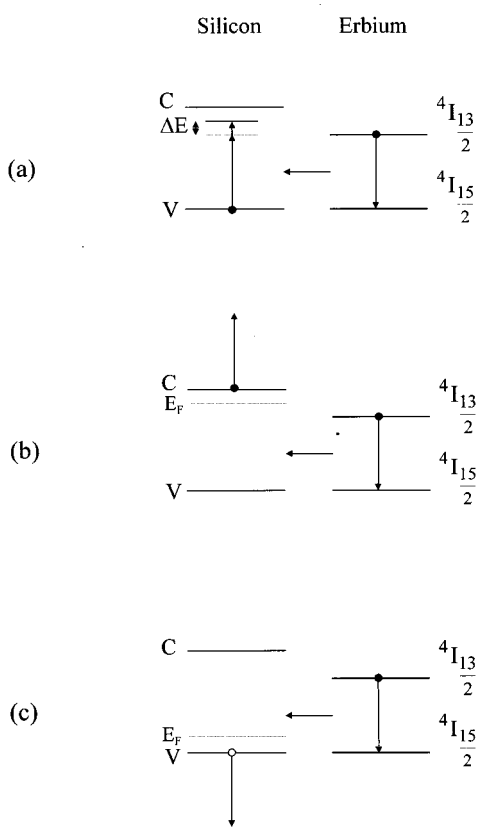

FIG. 1. Schematic representation of several possible nonradiative deexcitation processes for Er in Si: (a) the back transfer process, (b) Auger deexcitation with free electrons, and (c) with free holes.

These two deexcitation processes have been recently explored and some interesting features have been identified.[25–29] For instance, the back transfer has been verified by photocurrent measurements in Er-doped reverse biased diodes irradiated at 1.54 μm (Ref. 28) and by spectral response in Er-doped solar cells,[29] while the impurity Auger effect has been studied in Er-doped Si p-n junctions[27] and used in reverse biased LED's to achieve a fast switching of the electroluminescence signal.[25,26] However, a complete characterization of these phenomena is still missing. In particular, since both processes critically depend on free electrons and/or holes, an appropriate study has to be done at almost constant carrier concentrations. Such a study is lacking in the literature since the Er donor behavior results in a free-carrier concentration varying along its profile.

The situation is even more complicated in p-type material since the Er introduction produces compensation and formation of p-n junctions, so that, in the very same sample, Er atoms in p-type Si, in n-type Si, and in depletion regions are simultaneously present. The resulting luminescence behavior reflects all of these contributions: hence, nonradiative processes vary with the position of the Er site within the sample and it is therefore difficult to interpret the data. Finally, the role of bound carriers on the luminescence of Er in Si has never been properly assessed.

In the present paper we investigate in detail the excitation and deexcitation processes of Er^{3+} in Si doped with various concentrations of P or B. The doping is performed in such a

way to have almost uniform free-electron or hole concentrations in the Er-doped region. Under these circumstances the deexcitation phenomena of Er^{3+} involving free and bound carriers can clearly be evidenced and quantitatively analyzed. The results allowed us to obtain a clear picture of the several deexcitation processes.

II. EXPERIMENT

Samples were prepared by performing multiple P (or B) implants into a (100)-oriented *n*-type (or *p*-type) Czochralski (CZ) Si substrate ($\sim 4\ \Omega$ cm) in order to obtain a constant dopant concentration (ranging between 4×10^{16} and $1.2\times10^{18}/cm^3$) at depths between 0.5 and 2.5 μm. After implantation the samples were annealed at 1000 °C for 30 s in N_2 flux in order to remove the implantation damage and to activate the dopant.

All of these samples were then implanted with 4 MeV Er to a dose of $3.3\times10^{13}/cm^2$. The energy of the implant was chosen so that the Er profile is located in the region where the dopant profile is uniform. Also CZ Si substrates of *n* type and *p* type, $\sim 4\ \Omega$ cm, without previous P (or B) implantations, were implanted with Er for comparison. The Er dose was chosen in order to have an Er peak concentration of $5\times10^{17}/cm^3$ [below the threshold for the onset of Er precipitation in CZ Si (Ref. 30)]. After this implant the samples were annealed at 900 °C for 30 min in N_2 flux.

Chemical profiles were measured by secondary ion mass spectrometry (SIMS) using a CAMECA IMS 4*f* instrument. The Er profile was measured by using a 5.5-keV O_2^+ primary-ion beam and detecting the $^{168}Er^+$ signal. In order to avoid interferences with the $^{28}Si_6^+$ signal, a high-mass resolution ($\Delta M/M\sim1/3000$) was used, thus allowing minimum detectability limits in the 10^{13} atoms/cm^3 range.

The electrical activation of the implanted samples was measured by spreading resistance profiling (SRP). Samples for SRP were beveled at an angle of 17′. Spreading resistance data were converted into resistivity and then carrier concentration using calibrated samples and a computational procedure by Berkowitz and Lux.[35]

Photoluminescence (PL) measurements were performed by pumping with the 488-nm line of an Ar^+ ion laser. The pump power was varied between 0.01 and 200 mW over a circular area with a 1 mm diameter and the laser beam was mechanically chopped at 55 Hz. The luminescence signal was analyzed with a monochromator and detected with a liquid-nitrogen-cooled Ge detector. Spectra were recorded using a lock-in amplifier with the chopper frequency as a reference. Luminescence lifetime measurements were performed by monitoring the decay of the PL signal at 1.54 μm after pumping to steady state and mechanically switching off the laser beam. The overall time resolution of our system is of 30 μs. Low-temperature measurements were performed by using a closed-cycle liquid-He cooler system with the samples kept in vacuum.

III. RESULTS AND DISCUSSION

A. Carrier concentration

In Fig. 2 we report the carrier concentration profiles as obtained by SRP for a 4-MeV 3.3×10^{13} Er/cm^2 implantation

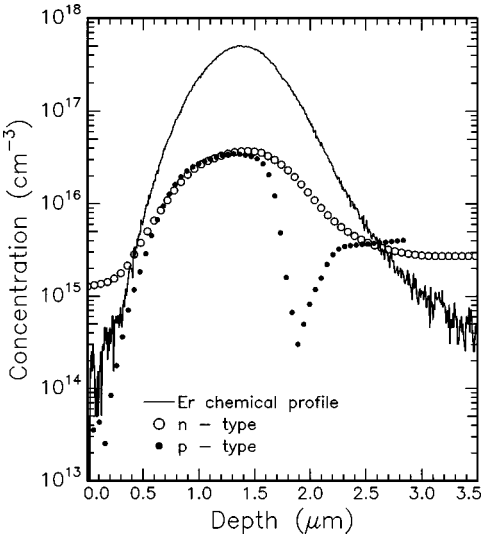

FIG. 2. Carrier concentration profiles of a 4-MeV Er implant to a dose of $3.3\times10^{13}/cm^2$ as measured by spreading resistance profiling in *n*-type $\sim 4\ \Omega$ cm CZ Si (○) and *p*-type $\sim 4\ \Omega$ cm CZ Si (●). Also reported is the erbium chemical profile as measured by SIMS (continuous line).

in *n*-type (open circles) and *p*-type (solid circles) $\sim 4\ \Omega$ cm CZ Si after annealing at 900 °C for 30 min. The Er chemical profile for these samples, as obtained by SIMS analyses, is also reported as a continuous line. Due to the fact that Er behaves as a donor in Si, the carrier concentration profile for Er-implanted *p*-type Si (solid circles) is quite complex. In fact, it consists of a *p*-type region just below the surface followed by a *p*-*n* junction at $\sim 0.2\ \mu$m, an *n*-type zone between 0.2 and 1.8 μm due to the donors introduced by Er, a second junction at $\sim 1.8\ \mu$m, and finally the *p*-type substrate. Therefore in the very same sample we have simultaneously Er atoms in *p*-type, *n*-type, and depletion regions.

In contrast, when implanting Er in *n*-type CZ Si (open circles), the sample is all *n*-type but the free-electron concentration profile follows that of Er so that we have regions with different electron concentrations. It should be noted that the maximum free-electron concentration is $4\times10^{16}/cm^3$ for both *n*-type and *p*-type materials and is about one order of magnitude lower than the implanted Er concentration. This is due to the fact that the electrical activity of Er in Si depends on the amount of O present in the sample. In particular it has been demonstrated that for Er implantation in CZ Si a maximum concentration of $\sim 4\times10^{16}/cm^3$ free electrons[21,23] is achieved; this electrical activity is limited by the O content and can be increased only by introducing more O in the substrate.[23]

In order to avoid the formation of junctions and to have almost uniform concentrations of electrons or holes in the region where Er sits, multiple P or B implants have been performed together with the Er implant and the carrier concentration profiles of these two sets of samples are reported in Fig. 3 and Fig. 4, respectively. The Er chemical profiles (4 MeV 3.3×10^{13} Er/cm^2 in all cases) as obtained by SIMS are also shown as a continuous line for comparison. Open circles refer to carrier concentration on samples implanted solely with the dopant, while closed circles are the results after the additional Er implant and annealing.

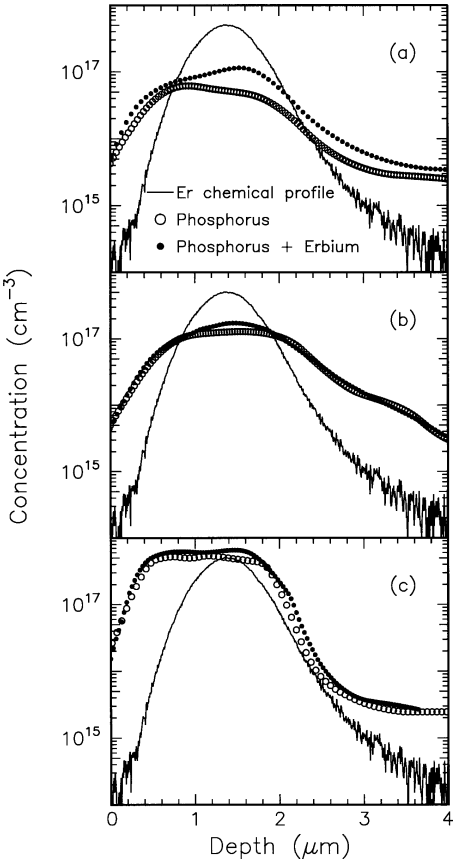

FIG. 3. Carrier concentration profiles as measured by spreading resistance for CZ-Si $\sim 4\,\Omega$ cm n-type samples implanted with P (○) to concentrations of 4×10^{16}/cm^3 (a), 1×10^{17}/cm^3 (b) and 4×10^{17}/cm^3 (c). Modification of the carrier concentration profiles after additional implantation with 4-MeV 3.3×10^{13} Er/cm^2 is also shown (●). The Er chemical profile as obtained by SIMS analysis is reported as a continuous line.

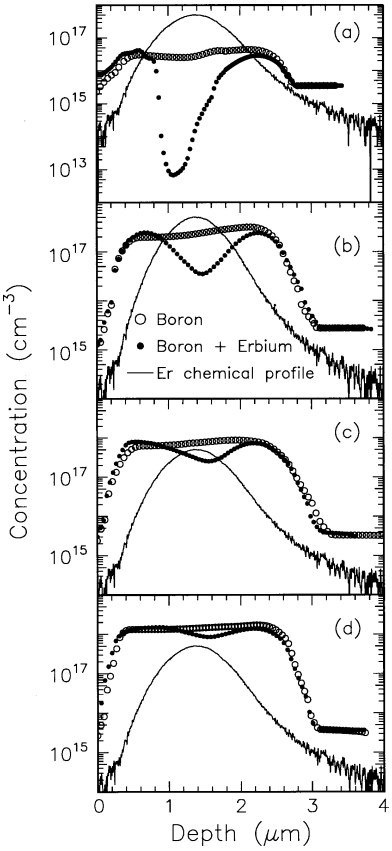

FIG. 4. Carrier concentration profiles as measured by spreading resistance for CZ Si $\sim 4\,\Omega$ cm p-type samples implanted with B (○) at concentrations of 5×10^{16}/cm^3 (a), 3×10^{17}/cm^3 (b), 6×10^{17}/cm^3 (c), and 1.2×10^{18}/cm^3 (d). Modifications of the carrier concentration profiles after additional implantation with 4-MeV 3.3×10^{13} Er/cm^2 is also shown (●). The Er chemical profile as obtained by SIMS analysis is reported as a continuous line.

Figure 3 reports the data on samples in which an almost constant concentration of P of 4×10^{16}/cm^3 (a), 1×10^{17}/cm^3 (b), and 4×10^{17}/cm^3 (c) has been realized. The additional Er implants slightly modify the total carrier concentration, which is seen to increase in all of these samples (as a result of a sum of donors introduced by P and by Er). This effect is very clear for the lowest P concentration while it is less evident as the P concentration increases. In all cases Er is embedded in n-type regions with almost constant carrier concentrations within the region where Er sits. Moreover three different carrier concentrations (spanning one order of magnitude) are obtained. Therefore these samples represent a good set to study the role of electrons on Er deexcitation processes.

The situation is more complicated in p-type samples. Figure 4 shows the hole concentrations on four samples implanted with constant B concentrations of 5×10^{16}/cm^3 (a), 3×10^{17}/cm^3 (b), 6×10^{17}/cm^3 (c), and 1.2×10^{18}/cm^3 (d) prior (open circles) and after (solid circles) Er introduction. The presence of Er produces a dramatic modification in the hole profiles with a large reduction in the regions of the Er peak. This effect is particularly strong for the lowest B concentration (5×10^{16} B/cm^3) for which the hole content in this region is decreased by 4 orders of magnitude. It is important to note that, in spite of this reduction, all of these samples remained p-type and no junction or n-type region exists. Note, however, that the decrease in hole concentration is not the same in all samples and does not correspond to the Er donor concentration. For instance, for 5×10^{16} B/cm^3 the decrease is by $\sim5\times10^{16}$/cm^3, for 3×10^{17} B/cm^3 it is by $\sim2.5\times10^{17}$/cm^3, and for 6×10^{17} B/cm^3 it is by $\sim4\times10^{17}$/cm^3. This suggests that the observed effect, rather than being due only to a partial B compensation caused by the donor character of Er, could be associated, especially for the higher B concentrations, to partial B deactivation caused by the formation of Er-B complexes. As the B concentration increases, the amount of Er-B complexes also increases (deactivating B) and their maximum amount corresponds to the peak Er concentration ($\sim4\times10^{17}$/cm^3). This scenario is also confirmed by the photoluminescence measurements on these samples that will be presented in Sec. III B.

In spite of the nonuniform hole profiles, the samples that we have prepared represent a set in which Er is completely embedded in p-type Si (no n-type region or junction exist) and it experiences an environment with the free-hole concentration varying by several orders of magnitude in the different samples. This set of samples can therefore be used to study nonradiative deexcitation processes of Er^{3+} as a function of hole concentration.

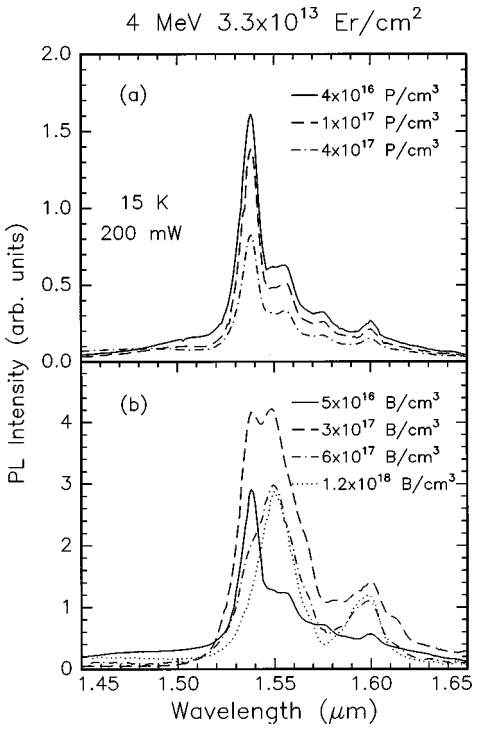

FIG. 5. Photoluminescence spectra for the samples implanted with 4 MeV 3.3×10^{13} Er/cm^2 and different P (a) or B (b) concentrations. Spectra were taken at 15 K and at a pump power of 200 mW.

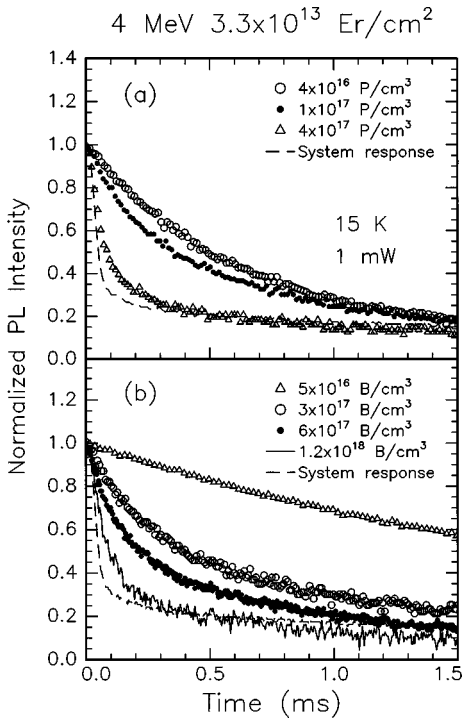

FIG. 6. Time decay of the 1.54-μm luminescence in the sample co-implanted with 4 MeV 3.3×10^{13} Er/cm^2 and several P (a) or B (b) concentrations. Data are taken at 15 K after shutting off a 1-mW pump pulse and are normalized to the initial value.

B. Photoluminescence

Figure 5 shows the photoluminescence spectra for the samples coimplanted with Er and P (a) or B (b) at different doping contents. Spectra were taken at 15 K and at a pump power of 200 mW.

In the case of phosphorus doping the PL spectra show the typical signal of Er^{3+} with the most intense peak at 1.538 μm and some other peaks at higher wavelengths. These peaks are all related to transitions among the $^4I_{13/2}$ and $^4I_{15/2}$ multiplets of Er^{3+} resulting from the splitting of the degenerate levels caused by the interaction with the crystalline field. The most intense signal is observed for the lowest P doping level with the intensity decreasing as the doping is increased. This suggests that, even at this low temperature, doping plays a role on the excitation and deexcitation processes of Er^{3+}.

In Fig. 5(b) spectra for different B concentrations are shown. First of all it is clear that the PL intensity is much higher with respect to the previous case [note that the vertical scales of Fig. 5(a) and Fig. 5(b) are different]. In the sample with 5×10^{16} B/cm^3 the shape of the spectrum is similar to those reported for n-type Si with the most intense peak at 1.538 μm. As the B concentration is increased, however, another peak at 1.55 μm takes over and eventually it becomes the dominant peak at the highest B values. This clear change in the shape of the PL spectrum is an indication that the surrounding of the emitting Er^{3+} centers has changed. This observation in the case of B doping had been previously made by Michel *et al.*[15] and strongly supports the idea that Er-B complexes formed with a consequent B deactivation.

In order to understand the role of doping on the luminescence of Er in Si, PL time decay measurements of the signal at ~1.5 μm have been performed at 15 K in these samples and the results are reported in Fig. 6. The measurements have been performed with a pump power of 1 mW to have a negligible contribution of the electrons and holes generated by the laser beam. The PL intensities are normalized to the initial value after the pump pulse was shut off at $t=0$. It is interesting to note that there is a clearly different effect of the dopant concentration on the time decay curves obtained in n-type (a) and p-type (b) Si. In fact, the PL signal in the n-type material decays very rapidly with P concentration. The lifetime of the excited state is 500 μs for 4×10^{16} P/cm^3 while it decreases to ~100 μs at 4×10^{17} P/cm^3. This means that in these samples strong nonradiative decay processes are present even at very low temperatures. The PL signal decays much more slowly in p-type Si. For instance, at 5×10^{16} B/cm^3 we obtain a PL lifetime of ~2 msec at 15 K. This lifetime is, to our knowledge, the longest ever observed for Er in Si and very likely it corresponds to the spontaneous radiative decay. As the B concentration is increased the lifetime decreases and reaches a value of ~150 μs at 1.2×10^{18} B/cm^3. Since at 15 K free carriers are frozen, these measurements demonstrate that bound holes and bound electrons play a role in quenching the luminescence of Er in Si.

Auger processes with bound carriers to shallow donors have been previously observed for Gd^{3+} in CdF_2,[36] Mn^{2+} in CdF_2,[37] and Yb^{3+} in InP,[38,39] and they have been theoretically discussed by Langer.[36,37,40] They consist in a nonradiative relaxation of the excited impurity center with the energy given to the bound electron.

Though the theory of energy transfer to bound carriers does not lead to a simple final formula, in order to have a

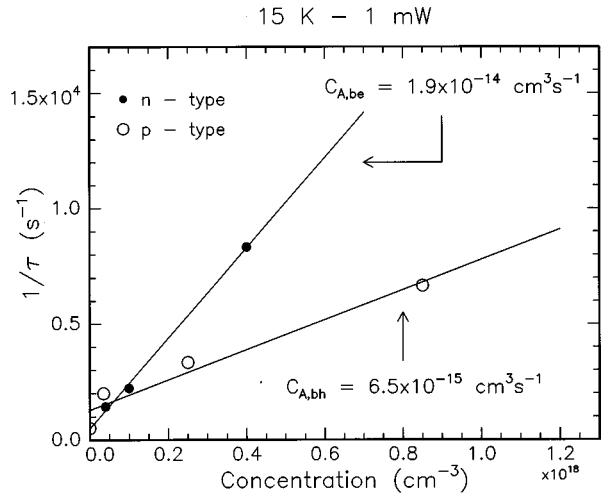

FIG. 7. Reciprocal of the time decay of the 1.54-μm luminescence for Er in n-type and p-type Si as a function of P (B) concentration. Data are extracted from Fig. 6.

figure on the strength of this effect we have used the data of Fig. 6 to calculate the effective Auger coefficients $C_{A,be}$ and $C_{A,bh}$ for localized bound electrons and bound holes, respectively. In Fig. 7 we report the reciprocal of the time decay at 1.54 μm as a function of P or B concentration, for n-type and p-type samples, respectively. In the case of p-type Si the horizontal scale has been chosen by taking into account only those B atoms not embodied into Er-B complexes. Their concentration has been assumed equal to the concentration of free holes measured by spreading resistance at room temperature. Furthermore, since as shown in Fig. 4 the hole concentration is not constant in the sample, the value corresponding to the position of the Er peak concentrations has been shown. This choice was motivated by the fact that in each sample the minimum concentration of free B in each sample corresponds to the position of the Er peak concentration. Hence, in the luminescence yield the tails of the profile give a minor contribution both because the Er content is small and because the nonradiative deexcitation processes there are more efficient. As a result of these considerations most of the signal in these samples comes from the peak of the profiles.

The data show a linear trend according to the expression $1/\tau = C_{A,b}N$, N being the shallow level concentration (P or B). The slopes give an effective Auger coefficient $C_{A,be} = 1.9\times10^{-14}$ cm^3 s^{-1} and $C_{A,bh} = 6.5\times10^{-15}$ cm^3 s^{-1} for bound electrons and bound holes, respectively. Auger deexcitation with bound carriers is therefore slightly stronger for bound electrons with respect to bound holes. These data will be compared with the Auger coefficient with free carriers.

C. Auger deexcitation with free carriers

We have also characterized the nonradiative decay of excited Er ions due to an Auger process with the energy transferred to free carriers. As soon as the temperature is increased above 15 K, shallow donors (or acceptors) ionize and free carriers are introduced in the conduction (or valence) band. The Er^{3+} Auger deexcitation with free carriers can therefore be characterized by measuring the decay lifetime, after excitation at low pump powers, under different situations: (a) at a fixed temperature and as a function of dopant (and hence free carrier) concentration; (b) at a fixed dopant concentration as a function of temperature. We have used both of these two methods and for both n-type and p-type samples. The results are summarized on Fig. 8 and Fig. 9 for n-type and p-type samples, respectively. All data were taken at 1 mW to reduce the effect of free carriers generated by the pumping laser beam.

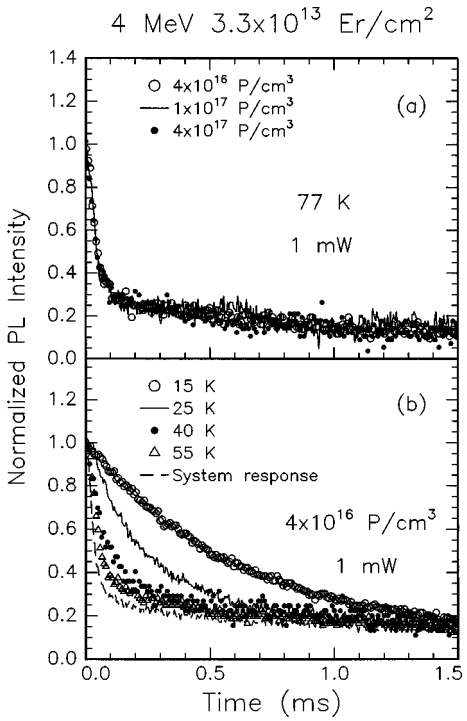

FIG. 8. Time decay of the 1.54-μm luminescence measured at 77 K in samples coimplanted with 4 MeV 3.3×10^{13} Er/cm^2 and several P concentrations (a). The time decay curves measured at different temperatures in the sample co-implanted with Er and 4×10^{16} P/cm^3 are also reported (b). Data were taken at a pump power of 1 mW.

In the n-type materials all of the decay curves measured at 77 K for samples containing different P concentrations [Fig. 8(a)] are resolution limited, suggesting that free electrons introduced in the conduction band produce a very efficient quenching of the Er^{3+} luminescence via an impurity Auger process. If now we keep the P concentration fixed [e.g., 4×10^{16} P/cm^3, see Fig. 8(b)] and slowly release electrons to the conduction band by increasing the temperature from 15 K step by step, we observe that the time decay decreases very fast upon increasing temperature and already approaches the system response time at temperatures above 55 K. These data confirm the relevant role of free electrons on Er^{3+} luminescence quenching. Note that quantitative information on the Auger process strength can only be obtained from the data of Fig. 8(b).

The situation appears to be different in p-type material (Fig. 9), where the effects of both temperature and dopant concentration on time decay appear to be much weaker. Time-decay curves at 77 K slowly decrease as a function of B concentration [Fig. 9(a)] and only approach the system response time at a B concentration of 1.2×10^{18}/cm^3. Furthermore, time decays for a sample doped with 3

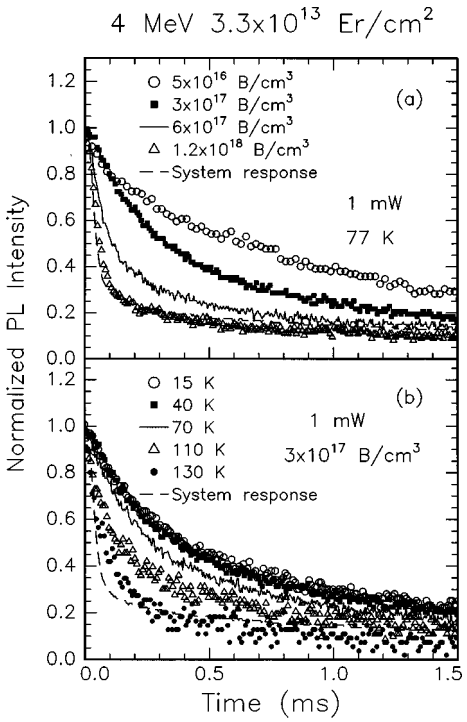

FIG. 9. Time decay of the 1.54-μm luminescence measured at 77 K in samples co-implanted with 4 MeV 3.3×10^{13} Er/cm^2 and several B concentrations (a). The time decay curves measured at different temperatures in the sample co-implanted with Er and 3×10^{17} B/cm^3 are also reported (b). Data were taken at a pump power of 1 mW.

$\times10^{17}$ B/cm^3 exhibit no change from 15 K up to 40 K and only at higher temperatures are seen to decrease [Fig. 9(b)]. At 130 K the lifetime is ~100 μs and only at higher temperatures does it become resolution limited. Note that for p-type samples information of the Auger strength can be obtained from both Fig. 9(a) and Fig. 9(b).

In order to understand the reasons for the different behavior in p-type and n-type samples we have reported in Fig. 10 the lifetime τ as extracted from the fits to the data of Fig. 8(b) and Fig. 9(b) as a function of temperature. It is interesting to note that the two samples we are comparing (4×10^{16} P/cm^3 and 3×10^{17} B/cm^3), in spite of the different doping concentration, are characterized by a similar carrier (electrons or holes) concentration in the Er peak region at room temperature (see Figs. 3 and 4). The data of Fig. 10 clearly show that the lifetime decreases much faster in n-type Si than in p-type Si as the temperature is increased, suggesting that nonradiative decay processes are either more severe or set in at a lower temperatures in n-type material.

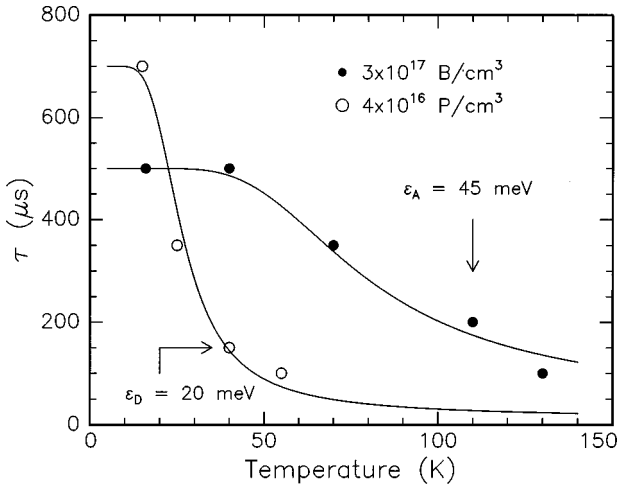

FIG. 10. Lifetime of the Er^{3+} excited state τ as extracted from the data in Fig. 8(b) and Fig. 9(b) vs temperature. Continuous lines show that the deexcitation occurs with well-defined activation energies associated with free carriers release from shallow levels.

If the process responsible for the fast quenching of the Er PL is an Auger with free carriers, we expect to have for n-type and p-type materials, respectively,

$$\frac{1}{\tau}=\frac{1}{\tau_0}+C_{A,e}n, \tag{1a}$$

$$\frac{1}{\tau}=\frac{1}{\tau_0}+C_{A,h}p, \tag{1b}$$

where τ is the PL decay lifetime, τ_0 the lifetime when carriers are frozen, $C_{A,e}$ and $C_{A,h}$ the Auger coefficient for electrons and holes, and n and p the free-electron and free-hole concentrations.

The release of free carriers from shallow levels is approximately described by

$$n\cong\frac{1}{\sqrt{2}}(N_dN_c)^{1/2}\exp\left(-\frac{\varepsilon_d}{2kT}\right), \tag{2a}$$

$$p\cong\frac{1}{\sqrt{2}}(N_aN_v)^{1/2}\exp\left(-\frac{\varepsilon_a}{2kT}\right), \tag{2b}$$

where N_d (N_a) is the concentration of donors (acceptors), N_c (N_v) is the density of states in the conduction (valence) band, and $\varepsilon_d(\varepsilon_a)$ is the energy of the shallow donor (acceptor) level.

By putting together Eqs. (1) and (2) one expects that, if τ versus T is dominated by an impurity Auger effect with free carriers, its temperature dependence will be approximately

$$\tau=\frac{1}{1/\tau_0+A\ \exp(-\varepsilon/2kT)} \tag{3}$$

where A is a constant and ε is the energy of the shallow donor (acceptor).

It is interesting to note that data in Fig. 10 can be nicely described by Eq. (3) with activation energies of 20 meV for n-type Si and 45 meV for p-type Si (continuous lines). The energy of 45 meV corresponds exactly with the acceptor level of B in Si, suggesting that the observed phenomenon is indeed a nonradiative Auger deexcitation of the Er^{3+} ions with holes in the valence band. More intriguing are the data of n-type Si since also the donor level of P has an energy of 45 meV while time decay shows an activation energy of 20 meV. Indeed, it is known that Er in the presence of oxygen acts as a donor introducing a shallow level at ~20 meV.[41] It is clear that electrons bound to this level will thermalize to the conduction band at temperatures much lower than those bound to P. Therefore we attribute the temperature depen-

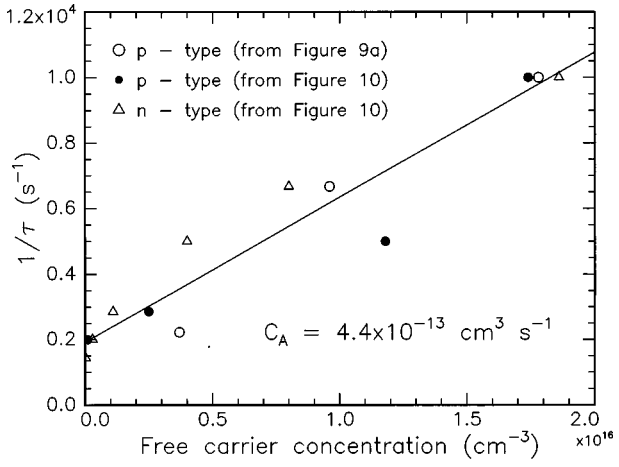

FIG. 11. Reciprocal of the decay lifetime of the PL signal at 1.54 μm (as obtained by fitting the time-decay curves) as a function of the free-carrier concentration (as obtained by calculations). Data for both electrons and holes are shown. An Auger coefficient of 4.4×10^{-13} cm^3 s^{-1} is obtained from the slope.

dence of the *n*-type data in Fig. 10 to the impurity Auger effect with free electrons released directly by Er donors.

These observations clarify the different behavior of Er^{3+} in *n*-type and *p*-type Si. In fact, in both cases nonradiative Auger deexcitation with free electrons or holes occurs. However, in *n*-type Si the effect appears particularly severe because electrons thermalizing from Er donors start to be released at very low temperatures affecting the PL lifetime. In *p*-type Si part of the B is deactivated by the presence of Er strongly reducing the concentration of acceptor levels; moreover, due to the B energy level, holes are released to the valence band at higher temperatures and hence the nonradiative deexcitation of Er^{3+} becomes severe only at higher temperatures.

The data of Fig. 8 and Fig. 9 can be used to obtain a quantitative estimate of the Auger coefficient of the Er^{3+} deexcitation with free carriers. In order to do this we have calculated, according to Eqs. (2a) and (2b), the concentration of free electrons (holes) for each temperature and dopant concentration at which measurements reported in Fig. 10 (for *n*-type and *p*-type Si) and Fig. 9(a) (for *p*-type Si) were performed. In the case of *n*-type Si the presence of both Er (4×10^{16}/cm^3 with a level at 20 meV from the conduction band) and P (with a level at 45 meV) has been taken into account. In *p*-type Si only the B atoms not embodied into Er-B complexes (as extracted from spreading resistance profiling at room temperature) have been considered. In Fig. 11 we report the reciprocal of the time decay as a function of free-carrier concentration for both *n* (open triangles) and *p*-type Si. For *p*-type Si, data from both Fig. 10 (solid circles) and Fig. 9(a) (open circles) are reported. It is interesting to note that all of the data for both electrons and holes lie on a single straight line with an Auger coefficient $C_{A,e}=C_{A,h}=(4.4\pm2)\times10^{-13}$ cm^3 s^{-1}.

Auger deexcitation to free carriers has been described theoretically by Langer[36,37,40] and Allen[42] and it has been observed in several systems.[27,36,37,43,44] According to the Langer theory the Auger coefficient in Eq. (1) has the following expression:

$$C_{A,e}=\frac{1}{\tau_{\rm rad}}\frac{1}{n_0} \tag{4}$$

where $\tau_{\rm rad}$ is the radiative lifetime of the impurity under investigation and n_0 a critical concentration given by

$$n_0=4\pi^{5/2}n_r^5\left[\frac{m_0}{m^*}137a_0\right]^{1/2}\lambda_0^{-7/2}, \tag{5}$$

where n_r is the refractive index of the host matrix, m_0 and m^* are the electron mass and the effective mass, respectively, a_0 is the Bohr radius, and λ_0 is the wavelength of the impurity emission. In the case of Er in Si, using $\tau_{\rm rad}=2$ msec we obtain $n_0=7\times10^{14}$ cm^{-3} and therefore $C_{A,e}\sim7\times10^{-13}$ cm^3/s in good agreement with our experimental findings. A similar value was recently estimated, on the basis of experimental results, for Er deexcitation with free electrons by Palm *et al.*[27]

It is important to note that the Auger coefficient with free carriers is 2 orders of magnitude higher than that with bound carriers as theoretically predicted for other systems.[37,40]

D. Implications on erbium physics and device perspectives

The data reported in the preceding sections have several important implications. First of all they demonstrate that there is a strong coupling between free carriers and Er. On one hand this produces Auger deexcitation of excited Er^{3+}, while on the other it suggests that also the reverse process, i.e., impact excitation of the Er from energetic carriers, should be highly probable. We can calculate the cross section for Auger deexcitation as $\sigma_A=C_{A,e}/v_{\rm th}$, $v_{\rm th}$ being the thermal velocity. We obtain $\sigma_A\sim5\times10^{-20}$ cm^2. It is interesting to note that this value is three orders of magnitude smaller with respect to the measured cross section for impact excitation of Er in Si [$\sigma_{\rm imp}\sim6\times10^{-17}$ cm^2 (Ref. 25)]. This is unexpected since the two processes seem to be just the reverse of one another. On the other hand while deexcitation always involves a transition from the $^4I_{13/2}$ to the $^4I_{15/2}$ state, impact excitation with sufficiently energetic electrons can involve transitions from the ground state ($^4I_{15/2}$) to any of the higher states ($^4I_{13/2}$, $^4I_{11/2}$, $^4I_{9/2}$, etc.), provided that carriers are hot enough. A fast nonradiative deexcitation from the excited state to the first excited state will then occur. The cross section for impact excitation represents then the integral of the cross sections of several different transitions. Together with this observation it should be noted that the cross section for impact excitation and Auger deexcitation is also proportional to the density of states in the correspondent final carrier configuration. Hence impact excitation is proportional to the density of states close to the bottom of the conduction band while Auger deexcitation is proportional to the density of states ~0.8 eV above the bottom of the conduction band. The former is higher than the latter. These observations can explain why $\sigma_{\rm imp}>\sigma_A$. The implications of this result are enormous. In fact, $\sigma_{\rm imp}=\sigma_A$ would have implied that population inversion by impact excitation is impossible since very high excitation rates necessarily imply also very high deexcitation rates and, at most, only half of the Er could be excited, thus not allowing (also in principle) laser operation.

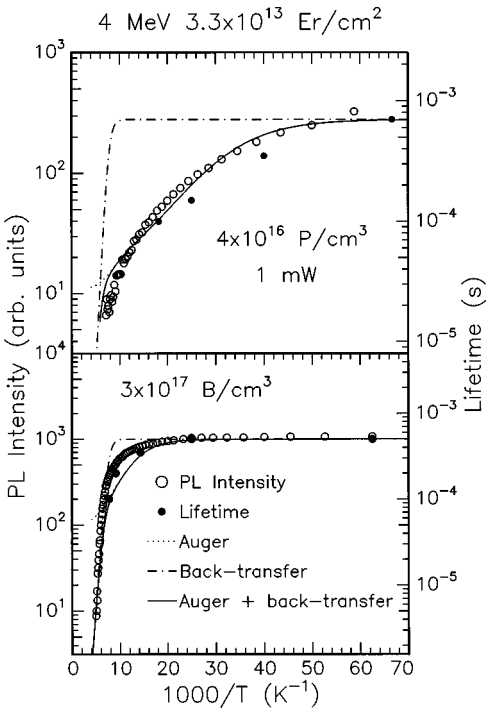

FIG. 12. Temperature dependence of the PL intensity at 1.54 μm (○) and of the lifetime (●) for the samples co-implanted with 4 MeV 3.3×10^{13} Er/cm^2 and 4×10^{16} P/cm^3 (a) or 3×10^{17} B/cm^3 (b). Data were taken at a pump power of 1 mW. Fits to the data by taking into account nonradiative Auger processes (dotted line), back-transfer process (dash-dotted line) and Auger+back-transfer (continuous line) processes are also shown.

The fact that $\sigma_{\rm imp}\gg\sigma_A$, instead, demonstrates that population inversion is achievable and a laser is, in principle, feasible.

We would like to note that the measured value of the Auger coefficient has other important implications on device operation. In fact, we[25,26] have recently shown that efficient and fast modulating LED's can be fabricated when exciting the Er ions within the depletion region of a reversed biased p^+-n^+ junction. During operation the Auger quenching is inhibited (within the depletion region) but it suddenly sets in when, at the diode turnoff, the depletion region shrinks and the excited Er ions find themselves embedded in a heavily doped n^+ region (with 1×10^{19} electrons/cm^3). The Auger coefficient we have determined now allows one to estimate that the luminescence lifetime at the switchoff of the diode will be of $\sim$200 ns and hence modulation frequencies of $\sim$5 MHz can be reached in the present device structures. By increasing the electron concentration to 2×10^{20}/cm^3 in the n^+ side of the device, frequencies of $\sim$100 MHz are achievable. This represents a quite interesting feature for device operation.

E. Deexcitation processes and luminescence intensity

In Fig. 12 we show the PL intensity taken at a pump power of 1 mW as a function of the reciprocal temperature for Er in both n-type Si (4×10^{16} P/cm^3) and p-type Si (3×10^{17} B/cm^3). In the same plot, as closed circles, we report the measured lifetime for both samples (right hand scale). In both cases the PL intensity and the associated lifetime are closely related. In n-type Si the PL intensity (and the lifetime) continuously decreases as the temperature is increased from 15 K towards higher values. The lifetime, however, can be measured up to 55 K since above it becomes resolution limited.

In p-type Si the Er luminescence and lifetime are both independent of temperature in the range from 15 to 40 K. However above 40 K an initially smooth and suddenly strong (above 130 K) temperature quenching occurs. In this latter case both luminescence and lifetime are seen to rapidly decrease with an activation energy of 0.15 eV. This regime is well known and has been attributed to energy back transfer.[20,27] In particular, since Er introduces a level in the Si band gap at $E_T=0.15$ eV from the bottom of the conduction band,[22] the extra energy necessary to complete the back-transfer will be

$$\Delta E=(E_G-E_T)-E_{\rm Er}=0.15\ {\rm eV}, \tag{6}$$

where E_G is the Si band gap and $E_{\rm Er}=0.8$ eV is the energy of the excited Er atom. Hence, the energy required for the back transfer process corresponds to the activation energy of the observed quenching. This process severely affects the luminescence yield up to room temperature.

In order to understand the behavior of the data in Fig. 12 it should be noted that all of the deexcitation processes directly affect the temperature dependence of the PL intensity. In fact, the PL intensity is given by

$$I_{\rm PL}\propto\frac{N_{\rm Er}^*}{\tau_{\rm rad}}, \tag{7}$$

where $N_{\rm Er}^*$ is the excited Er concentration and $\tau_{\rm rad}$ the radiative lifetime.

The excited Er concentration is, in general, obtained from the following rate equation:

$$\frac{dN_{\rm Er}^*}{dt}=\sigma_{eh}\phi(N_{\rm Er}-N_{\rm Er}^*)-N_{\rm Er}^*\left(\frac{1}{\tau_{bt}}+C_An+\frac{1}{\tau_0}\right), \tag{8}$$

where σ_{eh} is the excitation cross section through e-h recombinations, ϕ is the carrier flux, $N_{\rm Er}$ is the total Er concentration, τ_{bt} is the lifetime for the back transfer process, n is the electron concentration, and τ_0 is the lifetime below 15 K due to deexcitations with bound carriers. If the electron concentration introduced by the pumping laser is small, n in Eq. (8), and hence the Er lifetime, will be independent of ϕ. In this regime we can define

$$\frac{1}{\tau}=\frac{1}{\tau_{bt}}+C_An+\frac{1}{\tau_0}. \tag{9}$$

Under steady state conditions the rate equation (8) yields

$$N_{\rm Er}^*=\frac{\sigma_{eh}\phi\tau}{\sigma_{eh}\phi\tau+1}\,N_{\rm Er} \tag{10}$$

and, for small pump powers ($\sigma_{eh}\phi\ll1/\tau$)

$$N_{\rm Er}^*\cong\sigma_{eh}\phi\tau N_{\rm Er}. \tag{11}$$

Therefore, under these conditions, the luminescence intensity is

$$I_{\mathrm{PL}} \propto \frac{N_{\mathrm{Er}}^{*}}{\tau_{\mathrm{rad}}} = \sigma_{eh}\phi N_{\mathrm{Er}} \frac{\tau}{\tau_{\mathrm{rad}}}, \tag{12}$$

i.e., I_{PL} is proportional to the decay time. Any change in the decay time should then be reflected in the luminescence intensity.

The temperature dependencies for both p- and n-type Si can be therefore fitted inserting in Eq. (9) the measured Auger coefficient C_A, the calculated electron (hole) concentration versus temperature, the measured low-temperature lifetime τ_0 and describing the back transfer as

$$\frac{1}{\tau_{bt}} = W_0 \exp\left(-\frac{0.15\ \mathrm{eV}}{kT}\right), \tag{13}$$

where W_0 (the rate of the back transfer process) is the only fitting parameter. Fits to the data are also reported in Fig. 12 as a continuous line and show a very good agreement with the experimental data. The value of W_0 has been determined to be $1\times10^{9}\ \mathrm{s}^{-1}$. In the same figure, for clarity, we have also reported the effect of solely the back transfer (dot-dashed line) and the Auger (dotted line) processes. It is very clear that, in both p-type and n-type samples, back transfer alone cannot take into account the low-temperature quenching since it determines a quite sharp decrease starting from temperatures above 130 K. On the other hand Auger processes, while describing nicely the low-temperature data, result in a saturation at $\sim$150 K when most of the shallow levels are ionized and therefore cannot explain the higher-temperature quenching. Only a combination of both processes gives a nice explanation of the data.

A question naturally arises. What is going to happen if we increase the pump power. In this case we may enter a regime in which $\sigma_{eh}\phi > 1/\tau$ and hence we will have

$$I_{\mathrm{PL}} \propto \frac{N_{\mathrm{Er}}^{*}}{\tau_{\mathrm{rad}}} \cong \frac{N_{\mathrm{Er}}}{\tau_{\mathrm{rad}}}. \tag{14}$$

Therefore within this regime the PL intensity is not proportional to the Er lifetime and it assumes a constant value. However, since with increasing temperature τ decreases, in a measurement of the PL intensity versus $1/T$ at a fixed pump power, one can pass from a regime in which $\sigma_{eh}\phi > 1/\tau$ (at low temperatures) to a regime where $\sigma_{eh}\phi < 1/\tau$ (at high temperatures). The PL intensity versus $1/T$ reflects then two different regimes and special care should be taken in the interpretation of the data. This effect is clearly shown in Fig. 13 where we report the PL intensity versus the reciprocal temperature for Er in n-type Si (4×10^{16} P/cm^3) taken at 1 mW and at 200 mW. The two temperature dependencies show a completely different behavior. In fact, at 1 mW there is a continuous decrease in intensity as a result of donor ionization and nonradiative Auger deexcitation with free electrons. The PL intensity is then seen to vary by 2 orders of magnitude between 15 and 100 K in a fashion similar to the lifetime. In contrast, at 200 mW the PL intensity decreases only by less than a factor of 3 in the same temperature range. At higher temperatures, however, a strong decrease in the PL intensity occurs (with an activation energy of $\sim$0.15 eV) and the intensity is seen to decrease by 2 orders of magnitude between 100 K and room temperature. This decrease resembles that observed in p-type samples (Fig. 12), it has been reported several times in the literature[15,19,27,31,34] and it seems to be a quite common feature to all Er-doped Si samples, independent of the way of preparation.

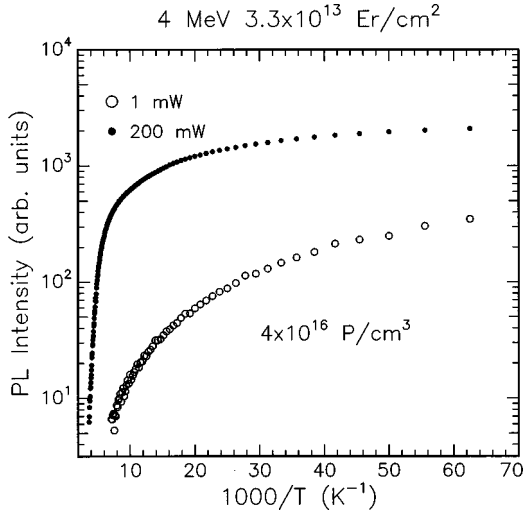

FIG. 13. Temperature dependence of the PL intensity at 1.54 μm for the sample co-implanted with 4 MeV 3.3×10^{13} Er/cm^2 and 4×10^{16} P/cm^3 at two different pump powers: 1 mW (○) and 200 mW (●).

Some controversy still exists in the literature on the mechanism producing this quenching. It has been attributed either to a decrease in the excitation cross section σ_{eh} or in the lifetime τ.[19,20,27] Indeed, I_{PL} is predicted to linearly depend on both σ_{eh} and τ [Eq. (12)]. From the data reported in Fig. 12 and Fig. 13 the following conclusions can be drawn. In p-type samples, where the 0.15 eV Er-related level is empty, τ is responsible for temperature quenching as also predicted earlier.[20,27] The nonradiative deexcitation process is the backtransfer schematically depicted in Fig. 1(a). In n-type Si, however, the situation is rather different. In this case, due to the short lifetime (below our detection resolution limit), it has been not possible to verify whether τ decreases in a fashion similar to I_{PL}. However, since we have observed the same quenching behavior even for the sample doped with 4×10^{17} P/cm^3, we can expect that the back transfer as depicted in Fig. 1(a) is unlikely to occur. In fact in n-type Si the level at 0.15 eV from the conduction band will mostly be full, and hence cannot accommodate an electron coming from the valence band. It has then been proposed[19] that, alternatively, the luminescence quenching with 0.15-eV activation energy might be due to a reduction in σ_{eh} as a result of the thermalization of an electron from the Er-related 0.15-eV level in the band gap to the conduction band. This process clearly affects the excitation efficiency (being excitation related to the recombination of an electron in this level with a hole in the valence band). Moreover, also this process is thermally activated with an activation energy of 0.15 eV.

We would like now to show that these two different points of view can be indeed reconciled. If we are in p-type Si the 0.15-eV level is empty and thus the back transfer process can occur. However, if the electron remains trapped in the Er-related level, Er excitation will occur again and the back transfer process would have had no effect. In order for the back transfer to be completed, thermalization of the elec-

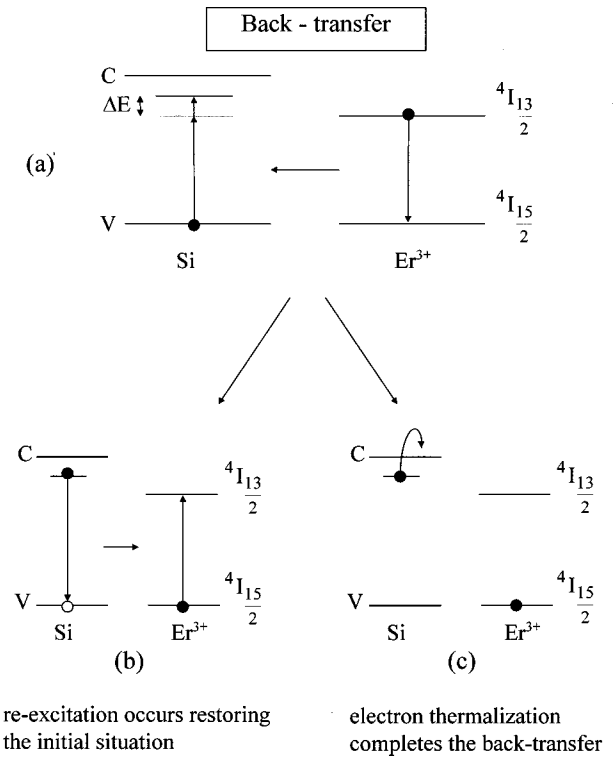

FIG. 14. Schematic picture of the back transfer process (a) and of the two possible processes that may occur after Er gives back the energy to the Si matrix: (b) the electron in the Er-related level recombines with a hole in the valence band causing the reexcitation of Er; (c) the electron in the Er-related level thermalizes in the conduction band and cannot excite Er.

tron in the trap level to the conduction band should necessarily occur. In this case the electron will become delocalized and the excited Er atom will be lost forever. The entire process is depicted in Fig. 14. Indeed, the direct evidences of the back transfer are all based on the generation of a photocurrent in Er-doped reverse-biased diodes irradiated at 1.54 μm,[28,29] demonstrating that the back transfer is always coupled to thermalization. Therefore, back transfer and thermalization represent indeed a single quenching process.

F. Excitation and quantum efficiency

All of the nonradiative deexcitation processes that we have investigated in this paper tend to decrease the luminescence efficiency for Er in Si. Efficiency is also affected by those processes producing *e-h* recombinations not ending up in Er excitation. We have seen that increasing the temperature nonradiative deexcitations increase (Auger and back transfer) and also excitation is affected (electron thermalization). The question is now what is the efficiency of the overall process under the best conditions (i.e., low temperatures). We can define three different efficiencies. The first one is the excitation efficiency, which is the ratio between the Er excitations occurring per unit area and time and the *e-h* pairs generated per unit area and time. Therefore this is a monitor of the probability of exciting Er. The second one is the internal quantum efficiency defined as the photons emitted by Er per unit area and time divided by the *e-h* pairs generated per unit area and time. Therefore this efficiency takes also

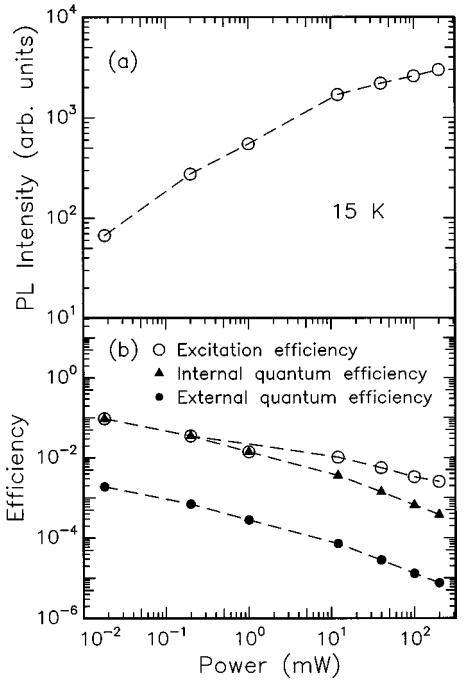

FIG. 15. Photoluminescence intensity at 1.54 μm measured at 15 K as a function of pump power for Er-doped Si (a). The pump power dependence of the excitation efficiency (○), internal quantum efficiency (▲), and external quantum efficiency (●) as extracted from (a) are shown in (b).

into account the probability that an Er atom, once excited, decays radiatively. Finally we have the external quantum efficiency, taking into account that, due to the difference in refractive indices between Si and air, only a fraction of the emitted photons is able to exit from the sample.

We have measured the pump power dependence of luminescence yield and time decay for Er (3.3×10^{13} Er/cm^2) in Si at 15 K for powers between 10 μW and 200 mW. The data of luminescence yield versus pump power are reported in Fig. 15(a). From these measurements the different efficiencies were derived by making comparison with an Er-implanted SiO_2 sample in which excitation by direct photon absorption occurs with a well-known cross section of $\sigma_{ph}=8\times10^{-21}$ cm^2.[45] In the calculation differences in the refractive indices between Si and SiO_2 were taken into account, lifetimes for the two samples were measured, and radiative lifetimes of 15 and 2 ms were assumed for Er in SiO_2 and in Si, respectively. Finally, for Er in Si it was assumed that each photon from the pump laser generates an *e-h* pair. The results are reported in Fig. 15(b). It is interesting to note that at low pump powers the excitation efficiency for Er in Si is 10%. This is evidence that at low temperatures and low pump powers competitive phenomena are not so important and a large fraction of *e-h* pairs produces Er excitation. Moreover, at low pump powers nonradiative decay processes are strongly reduced. If the measured 2-ms decay time corresponds indeed to the radiative lifetime (as we are assuming), then nonradiative processes are totally inhibited and also the internal quantum efficiency is 10%. This is a direct proof that Er luminescence in Si can be a very efficient process under appropriate circumstances. Note that this process in Si is orders of magnitude more efficient than in SiO_2. The

internal quantum efficiency for Er in SiO_2 at an equivalent Er dose (3.3×10^{13} Er/cm^2) would have been of only 2.5×10^{-7}. The very high efficiency of the luminescence of Er in Si is the result of an extremely efficient excitation. Indeed from these data we can estimate a cross section for excitation through the formula

$$\eta_i=\sigma_{eh}\phi_{\mathrm{Er}}\frac{\tau}{\tau_{\mathrm{rad}}}, \tag{15}$$

where η_i is the internal quantum efficiency, σ_{eh} is the cross section for excitation through e-h recombinations mediated by an Er-related level in the gap, and ϕ_{Er} is the areal density of Er. We obtain $\sigma_{eh}=3\times10^{-15}$ cm^2. This value is much higher than that obtained for impact excitation ($\sigma_{\mathrm{imp}}\sim6\times10^{-17}$ cm^2).[26] It is interesting to note that we have recently[26] measured the product $\sigma_{eh}\,\tau$ in forward biased operating Er-doped LED's at room temperature and we obtained a value of 6.5×10^{-22} cm^2 s. From the Auger coefficient measured in the present paper we can now estimate that the lifetime of the excited Er^{3+} is $\sim$200 ns in a device structure having 10^{19} electrons/cm^3. We can therefore extract $\sigma_{eh}\sim3\times10^{-15}$ cm^2. It is certainly noteworthy that similar cross sections have been obtained from independent sets of data in photoluminescence and forward bias electroluminescence. The excitation cross section for Er^{3+} in Si through carrier-mediated recombinations is about 7 orders of magnitude higher than that for Er^{3+} in SiO_2 through direct photon absorption.

In principle these data would suggest that, with $\sigma_{eh}\gg\sigma_{\mathrm{imp}}\gg\sigma_{ph}$, the most efficient way for pumping Er is under photoluminescence or forward bias electroluminescence. In contrast, it has been demonstrated[10,25] that reverse bias electroluminescence is by far more efficient. This is due to the fact that, despite the smaller excitation cross section (σ_{imp}), under reverse bias Er is pumped within a depletion region where Auger processes with free carriers are inhibited. In contrast, under forward bias in spite of the higher excitation cross section (σ_{eh}), Er is excited in a region full of free carriers and nonradiative phenomena make the overall luminescence process less efficient.

Figure 15 also shows that the efficiencies decrease with increasing pump power. This is not surprising since several competing phenomena set in as the power is increased. First of all, due to the limited amount of Er atoms, e-h recombination routes not producing Er excitations become increasingly more important. Furthermore, as the density of injected carriers increases, nonradiative Auger deexcitations will take place, further decreasing the overall efficiency.

The main message, however, is that under appropriate conditions the 1.54-μm luminescence of Er in Si can be an extremely efficient process. The challenge is now to reproduce these conditions in a working device operating at room temperature.

IV. CONCLUSIONS

We have studied the excitation and deexcitation processes of Er^{3+} in Si. Excitation is proposed to occur through the sequential capture of electrons and holes at an Er-related level in the Si band gap. The overall cross section for Er excitation through this process has been evaluated to be $\sim3\times10^{-15}$ cm^2, i.e., 7 orders of magnitude higher than direct photon absorption. This value is even higher than the cross section for excitation through impact with hot carriers ($\sigma_{\mathrm{imp}}\sim6\times10^{-17}$ cm^2) suggesting that excitation of Er^{3+} in Si is a very efficient process. Indeed, at low temperatures, where nonradiative deexcitation processes are inhibited, the internal quantum efficiency of Er luminescence in Si can be as high as $\sim$10%. However, as soon as the temperature is increased, several competing nonradiative processes take place. Among them we have identified the following.

(i) An Auger process with free electrons and free holes, dominating the quenching behavior at temperatures below $\sim$120 K and having an Auger coefficient of $\sim5\times10^{-13}$ cm^3/s.

(ii) An Auger process with localized electrons or holes that determine the nonradiative deexcitation processes at very low temperatures (below 15 K) and exhibiting an effective Auger coefficient 2 orders of magnitude lower than that of free carriers.

(iii) An energy back transfer process, dominating quenching behavior at temperatures above $\sim$120 K, consisting of 2 steps: a promotion of an electron from the valence band to an Er related level plus electron thermalization to the conduction band.

The strength of all of these nonradiative processes is crucially dependent on temperature, carrier concentration, and Er electrical behavior. Hence the pathways towards high efficiency of Er luminescence in Si requires properly engineered Er sites and/or proper device structure to reduce or inhibit these nonradiative processes. For instance, in photoluminescence and forward bias electroluminescence, in spite of the high excitation cross section (3×10^{-15} cm^2) both Auger processes with free carriers and energy back transfer will result in a strong temperature quenching limiting room-temperature performances. On the other hand, pumping through impact excitation in a depletion layer (in reverse bias electroluminescence) allows one to reduce the background free-carrier concentration during pumping, thus limiting nonradiative Auger processes. Therefore, in spite of the lower excitation cross section (6×10^{-17} cm^2) the overall room-temperature efficiency is higher in this last case. Moreover, Auger nonradiative deexcitation can be advantageously triggered in at the turnoff of the diode, allowing one to achieve modulation of the light emission at frequencies up to 100 MHz. These results open new perspectives in both understanding and applications of Er-doped silicon.

ACKNOWLEDGMENTS

We would like to acknowledge Alberto Decaro for participating in some of the experiments reported in this paper. We wish also to thank Emanuele Rimini for several useful discussions and his suggestions throughout the performance of this work. Aldo Spada and Antonio Marino are acknowledged for their expert technical assistance. This work has been supported in part by the European Esprit Project SCOOP (Silicon Compatible Optoelectronics) and in part by ''Progetto Finalizzato'' MADESS II.

[1] R. A. Soref, Proc. IEEE **81**, 1687 (1993).
[2] L. T. Canham, MRS Bull. **18**, 22 (1993); L. T. Canham, Phys. World **5**, 41 (1992).
[3] L. T. Canham, W. Y. Leong, M. I. J. Beale, T. J. Cox, and L. Taylor, Appl. Phys. Lett. **57**, 1046 (1990).
[4] L. Tsybeskov, K. L. Moore, D. G. Hall, and P. M. Fauchet, Phys. Rev. B **54**, R8361 (1996).
[5] S. Fukatsu, N. Usami, and Y. Shiraki, Appl. Phys. Lett. **63**, 967 (1993).
[6] *Rare Earth Doped Semiconductors*, edited by G. S. Pomrenke, P. B. Klein, and D. W. Langer. MRS Symp. Proc. No. 301 (Materials Research Society, Pittsburgh, 1993).
[7] *Rare Earth Doped Semiconductors II*, edited by S. Coffa, A. Polman, and R. N. Schwartz, MRS Symp. Proc. No. 422 (Materials Research Society, Pittsburgh, 1996).
[8] H. Ennen, J. Schneider, G. Pomrenke, and A. Axmann, Appl. Phys. Lett. **43**, 943 (1983).
[9] H. Ennen, G. Pomrenke, A. Axmann, K. Eisele, W. Haydl, and J. Schneider, Appl. Phys. Lett. **46**, 381 (1985).
[10] G. Franzò, F. Priolo, S. Coffa, A. Polman, and A. Carnera, Appl. Phys. Lett. **64**, 2235 (1994).
[11] B. Zheng, J. Michel, F. Y. G. Ren, L. C. Kimerling, D. C. Jacobson, and J. M. Poate, Appl. Phys. Lett. **64**, 2842 (1994).
[12] J. Stimmer, A. Reittinger, J. F. Nutzel, G. Abstreiter, H. Holzbrecher, and Ch. Buchal, Appl. Phys. Lett. **68**, 3290 (1996).
[13] O. B. Gusev, A. N. Kuznetsov, E. I. Terukov, M. R. Bresler, V. Kh. Kudoyarova, I. N. Yassievich, B. P. Zakharchenya, and W. Fuhs, Appl. Phys. Lett. **70**, 240 (1997).
[14] D. L. Adler, D. C. Jacobson, D. J. Eaglesham, M. A. Marcus, J. L. Benton, J. M. Poate, and P. H. Citrin, Appl. Phys. Lett. **61**, 2181 (1992).
[15] J. Michel, J. L. Benton, R. F. Ferrante, D. C. Jacobson, D. J. Eaglesham, E. A. Fitzgerald, Y. H. Xie, J. M. Poate, and L. C. Kimerling, J. Appl. Phys. **70**, 2672 (1991).
[16] A. Terrasi, G. Franzò, S. Coffa, F. Priolo, F. D'Acapito, and S. Mobilio, Appl. Phys. Lett. **70**, 1712 (1997).
[17] S. Coffa, F. Priolo, G. Franzò, V. Bellani, A. Carnera, and C. Spinella, Phys. Rev. B **48**, 11 782 (1993).
[18] R. Serna, M. Lohmeier, P. M. Zagwijn, E. Vlieg, and A. Polman, Appl. Phys. Lett. **66**, 1385 (1995).
[19] F. Priolo, G. Franzò, S. Coffa, A. Polman, S. Libertino, R. Barklie, and D. Carey, J. Appl. Phys. **78**, 3874 (1995).
[20] S. Coffa, G. Franzò, F. Priolo, A. Polman, and R. Serna, Phys. Rev. B **49**, 16 313 (1994).
[21] J. L. Benton, J. Michel, L. C. Kimerling, D. C. Jacobson, W. H. Xie, D. J. Eaglesham, E. A. Fitzgerald, and J. M. Poate, J. Appl. Phys. **70**, 2667 (1991).
[22] S. Libertino, S. Coffa, G. Franzò, and F. Priolo, J. Appl. Phys. **78**, 3867 (1995).
[23] F. Priolo, S. Coffa, G. Franzò, C. Spinella, A. Carnera, and V. Bellani, J. Appl. Phys. **74**, 4936 (1993).
[24] I. N. Yassievich and L. C. Kimerling, Semicond. Sci. Technol. **8**, 718 (1993).
[25] G. Franzò, S. Coffa, F. Priolo, and C. Spinella, J. Appl. Phys. **81**, 2784 (1997).
[26] S. Coffa, G. Franzò, and F. Priolo, Appl. Phys. Lett. **69**, 2077 (1996).
[27] J. Palm, F. Gan, B. Zheng, J. Michel, and L. C. Kimerling, Phys. Rev. B **54**, 17 603 (1996).
[28] J. Michel, B. Zheng, J. Palm, E. Ouellette, F. Gan, and L. C. Kimerling, in *Rare-Earth Doped Semiconductors*, edited by A. Polman *et al.*, MRS Symp. Proc. No. 422 (Materials Research Society, Pittsburgh, 1996), p. 317.
[29] P. G. Kik, M. J. A. de Dood, K. Kikoin, and A. Polman, Appl. Phys. Lett. **70**, 1721 (1997).
[30] D. J. Eaglesham, J. Michel, E. A. Fitzgerald, D. C. Jacobson, J. M. Poate, J. L. Benton, A. Polman, Y.-H. Xie, and L. C. Kimerling, Appl. Phys. Lett. **58**, 2797 (1991).
[31] A. Polman, J. S. Custer, E. Snoeks, and G. N. van den Hoven, Nucl. Instrum. Methods Phys. Res. B **80/81**, 653 (1993).
[32] H. Przybylinska, G. Hendorfer, M. Bruckner, L. Palmetshofer, and W. Jantsch, Appl. Phys. Lett. **66**, 490 (1995).
[33] A. Polman, G. van den Hoven, J. S. Custer, J. H. Shin, and R. Serna, J. Appl. Phys. **77**, 1256 (1995).
[34] H. Przybylinska, W. Jantsch, Yu. Suprun-Belevitch, M. Stepikhova, L. Palmetshofer, G. Hendorfer, A. Kozanecki, R. J. Wilson, and B. J. Sealy, Phys. Rev. B **54**, 2532 (1996).
[35] H. L. Berkowitz, and R. A. Lux, J. Electrochem. Soc. **18**, 1137 (1981).
[36] J. M. Langer and Le Van Hong, J. Phys. C **17**, L923 (1984).
[37] A. Suchocki and J. M. Langer, Phys. Rev. B **39**, 7905 (1989).
[38] K. Takahei, A. Taguchi, H. Nakagome, K. Uwai, and P. S. Whitney, J. Appl. Phys. **66**, 4941 (1989).
[39] A. Taguchi, M. Taniguchi, and K. Takahei, Appl. Phys. Lett. **60**, 965 (1992).
[40] J. M. Langer, J. Lumin. **40/41**, 589 (1988).
[41] L. Palmetshofer, Yu. Suprun-Belevich, and M. Stepikhova, Nucl. Instrum. Methods B **127/128**, 479 (1997).
[42] J. W. Allen, J. Phys. C **19**, 6287 (1986).
[43] S. G. Ayling and J. W. Allen, J. Phys. C **20**, 4251 (1987).
[44] P. B. Klein, J. E. Furneaux, and R. L. Henry, Phys. Rev. B **29**, 1947 (1984).
[45] K. Takahei and A. Taguchi, Mater. Sci. Forum **83–87**, 641 (1992).